

M3-Net: A Cost-Effective Graph-Free MLP-Based Model for Traffic Prediction

Guangyin Jin*
National Innovative Institute of
Defense Technology
jinguangyin18@nudt.edu.cn

Sicong Lai*
The Hong Kong University of Science
and Technology
slai892@connect.hkust-gz.edu.cn

Xiaoshuai Hao
Beijing Academy of Artificial
Intelligence
xshao@baai.ac.cn

Mingtao Zhang
Peking University
mingtaozhang@pku.edu.cn

Jinlei Zhang[†]
Beijing Jiaotong University
zhangjinlei@bjtu.edu.cn

Abstract

Achieving accurate traffic prediction is a fundamental but crucial task in the development of current intelligent transportation systems. The main challenges of the existing deep learning approaches are that they either depend on a complete traffic network structure or require intricate model designs to capture complex spatio-temporal dependencies. These limitations pose significant challenges for the efficient deployment and operation of deep learning models on large-scale datasets. To address these challenges, we propose a cost-effective graph-free Multilayer Perceptron (MLP) based model M3-Net for traffic prediction. Extensive experiments conducted on multiple real datasets demonstrate the superiority of the proposed model in terms of prediction performance and lightweight deployment. Our code is available at https://github.com/jinguangyin/M3_NET

CCS Concepts

• Information systems → Spatial-temporal systems.

Keywords

Traffic prediction, spatio-temporal modeling, multilayer perceptron

ACM Reference Format:

Guangyin Jin, Sicong Lai, Xiaoshuai Hao, Mingtao Zhang, and Jinlei Zhang. 2025. M3-Net: A Cost-Effective Graph-Free MLP-Based Model for Traffic Prediction. In *Proceedings of the 34th ACM International Conference on Information and Knowledge Management (CIKM '25)*, November 10–14, 2025, Seoul, Republic of Korea. ACM, New York, NY, USA, 5 pages. <https://doi.org/10.1145/3746252.3760815>

1 INTRODUCTION

Accurate traffic forecasting serves as the analytical backbone of intelligent transportation systems. Recent advances in spatio-temporal

*Both authors contributed equally to this research.

[†]Corresponding author

Permission to make digital or hard copies of all or part of this work for personal or classroom use is granted without fee provided that copies are not made or distributed for profit or commercial advantage and that copies bear this notice and the full citation on the first page. Copyrights for components of this work owned by others than the author(s) must be honored. Abstracting with credit is permitted. To copy otherwise, or republish, to post on servers or to redistribute to lists, requires prior specific permission and/or a fee. Request permissions from permissions@acm.org.
CIKM '25, Seoul, Republic of Korea.

© 2025 Copyright held by the owner/author(s). Publication rights licensed to ACM.
ACM ISBN 979-8-4007-2040-6/2025/11
<https://doi.org/10.1145/3746252.3760815>

(ST) models have significantly improved predictive accuracy by capturing how road segments interact and how these interactions evolve over time. However, modern urban networks are becoming increasingly large, dense, and noisy, widening the gap between laboratory benchmarks and real-world deployments.

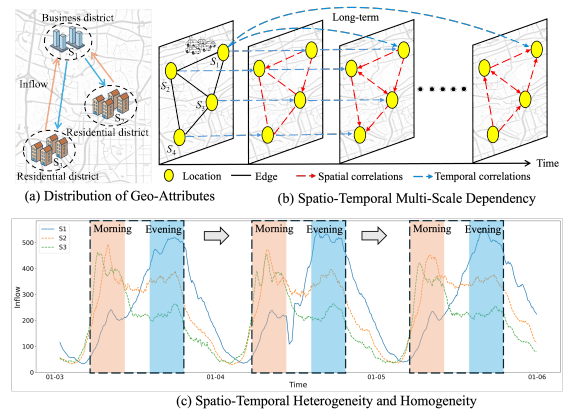


Figure 1: Spatio-Temporal Characteristics of Traffic Flow.

This deployment gap highlights the structural complexity of traffic flow data. As illustrated in Figure 1, although S2 and S3 are geographically apart, both belong to residential districts and exhibit highly similar inflow patterns during morning and evening rush hours, demonstrating spatial homogeneity. In contrast, S1, located in a business district, shows significantly higher and more volatile inflow peaks in the morning, highlighting spatial heterogeneity across regions with different functional roles. The coexistence of homogeneity and heterogeneity poses challenges for modeling. Moreover, Figure 1(b) illustrates the existence of complex multi-scale spatio-temporal dependencies in traffic flow. For example, a traffic disruption at node S1 may rapidly propagate to nearby nodes such as S2 and S3, and eventually extend to more distant areas like S4. This reflects both short-term local dependencies, characterized by immediate responses among adjacent regions, and long-term global dependencies, where the influence persists and spreads across space and time. Such patterns evolve dynamically across multiple spatial and temporal scales. Therefore, it is essential to build models that can handle both spatial diversity and multi-scale spatio-temporal dependencies for accurate traffic forecasting.

Recently, although there has been significant growth of works for urban traffic prediction as well as analogous ST forecasting tasks [6, 13], the aforementioned challenges are still not fully addressed.

Some methods focus on modeling ST correlations by utilizing a single shared model across all locations [8, 15, 23]. Such approaches often overlook the inherent heterogeneity among different regions and fail to explicitly capture diverse spatial-temporal interaction patterns, making it difficult for the model to adapt to varying local characteristics. Another line of research builds graph-structured representations to enhance spatial modeling [4, 5, 7, 10, 11, 19, 22], typically propagating information along static or learned graphs. While effective in representing spatial relations, these models heavily rely on predefined topologies and incur significant computational overhead, which limits scalability in dynamic or large-scale networks. More recently, attention-based methods have been developed to learn long-range ST dependencies in a fully data-driven manner without explicit graph construction [12, 17, 21]. Although these methods improve modeling flexibility, they still struggle to distinguish between local heterogeneity and global homogeneity and often suffer from high memory and computational costs, hindering their deployment in real-world traffic systems.

To address these challenges, we propose **M3-Net**, a novel and efficient ST forecasting framework based on a pure MLP architecture. In contrast to traditional graph-structured or attention-based methods, M3-Net learns ST dynamics directly from raw traffic sequences without relying on explicit road network topology construction, thereby significantly reducing model complexity and improving deployment friendliness. Specifically, M3-Net introduces two key components. First, for spatial modeling, M3-Net designs a **Spatial MLP** module equipped with **adaptive grouping matrices**, which flexibly captures heterogeneous local patterns as well as homogeneous global structures, thus unifying the learning of complex spatial properties. Second, for temporal modeling, M3-Net introduces a **Channel MLP** enhanced with a **Mixture-of-Experts (MoE)** mechanism, enabling dynamic capacity allocation to better capture multi-scale ST dependencies present in traffic flows. Through this novel architecture, M3-Net achieves a favorable balance between modeling expressiveness, computational efficiency, and generalization, enabling stable and robust forecasting performance across urban networks of varying scales and structural complexities.

2 METHODOLOGY

In this section, we introduce the proposed M3-Net framework, as illustrated in Figure 2. Concretely, M3-Net consists of four key building blocks as follows: 1) **Embedding Layer** fuses raw ST series with dedicated temporal (day-time & week-time) and node embeddings to provide context-rich token representations; 2) **M3 Layer** is composed of **Spatial MLP** and **Channel MLP**, where the Spatial MLP employs an adaptive grouping matrix to aggregate sensors into dynamic clusters and applies token mixing to capture inter-cluster interactions with residual refinement, the Channel MLP is with a MoE mechanism, enabling the model to learn heterogeneous feature dependencies while remaining lightweight; 3) **Regression Layer** performs linear projection to produce accurate multi-horizon traffic predictions.

2.1 Embedding Layer

To capture the complex spatio-temporal dependencies in traffic sequences, we embed the raw input data using a fully connected

layer. Given the historical traffic sequence $X_{t-L+1:t} \in \mathbb{R}^{L \times N \times C}$, where L is the sequence length, N is the number of nodes, and C is the number of input features. We obtain the dynamic feature embedding $E_F \in \mathbb{R}^{N \times D_F}$ via $E_F = \text{FC}(X_{t-L+1:t})$, where D_F is the projected feature dimension. To model node-specific static characteristics, we introduce a learnable spatial embedding $E_S \in \mathbb{R}^{N \times D_S}$. Meanwhile, to incorporate temporal periodicity, we construct two temporal embedding dictionaries: a time-of-day embedding matrix $E_d \in \mathbb{R}^{T_d \times D_d}$ and a day-of-week embedding matrix $E_w \in \mathbb{R}^{T_w \times D_w}$, where T_d and T_w denote the number of intervals in a day and week, respectively. The corresponding temporal embeddings are retrieved via index lookups: $E_T^{(d)} = E_d[\text{idx}_t^{(d)}] \in \mathbb{R}^{N \times D_d}$ and $E_T^{(w)} = E_w[\text{idx}_t^{(w)}] \in \mathbb{R}^{N \times D_w}$. Finally, we concatenate all embeddings along the feature dimension to form the complete spatiotemporal representation $H \in \mathbb{R}^{N \times D_H}$, where $H = E_F \parallel E_S \parallel E_T^{(d)} \parallel E_T^{(w)}$ and $D_H = D_F + D_S + D_d + D_w$.

2.2 MLP-Mixer with MoE

Spatial MLP. To model spatial dependencies among nodes, we introduce a Spatial MLP module equipped with an adaptive grouping mechanism. Given the input tensor $H \in \mathbb{R}^{N \times D}$, we generate an adaptive grouping matrix $G \in \mathbb{R}^{N \times g}$ to partition the N nodes into g groups. This matrix enables aggregation of node-level features into group-level representations via $H_g = G^T H \in \mathbb{R}^{g \times D}$, where G^T denotes the transpose of G . The grouped features are then passed through a shared MLP to capture intra-group patterns, yielding $\hat{H}_g = \text{MLP}(H_g) \in \mathbb{R}^{g \times D}$. These transformed features are subsequently mapped back to the original node space by multiplying with G , resulting in $\hat{H} = G \hat{H}_g \in \mathbb{R}^{N \times D}$. A residual connection is then added to preserve the original representation, giving the spatially enhanced output $H_s = H + \hat{H}$.

Channel MLP. To further capture nonlinear interactions along the feature dimension, we introduce a Channel MLP module with a Mixture-of-Experts (MoE) mechanism. The spatial-enhanced output $H_s \in \mathbb{R}^{N \times D}$ is first passed through a softmax-based gating network to compute expert weights $\alpha = \text{SoftmaxGate}(H_s) \in \mathbb{R}^{N \times K}$, where K denotes the number of experts. Each expert MLP_k independently processes the same input to produce $O_k = \text{MLP}_k(H_s) \in \mathbb{R}^{N \times D}$ for $k = 1, \dots, K$. These outputs are then weighted and combined using the gating scores, resulting in the final output representation $H_c = \sum_{k=1}^K \alpha_k \odot O_k$, where \odot denotes element-wise multiplication.

2.3 Regression Layer

After embedding layer and M3 layer, we obtain a representation tensor $H_c \in \mathbb{R}^{N \times D}$ enriched with deep spatio-temporal dependencies. The prediction head is responsible for transforming this latent representation into the final forecasting output. The final forecasting output is thus computed as $\hat{Y}_{t:t+F} = \text{FC}_{\text{regression}}(H_c)$.

3 EXPERIMENTS

3.1 Experimental Setup

We evaluate our model on four normal datasets and three large-scale datasets. The normal datasets include PEMS03, PEMS04, PEMS07 and PEMS08, Which are collected from California highways [16]. In the experiments, we use the traffic flow of the last 12 time steps

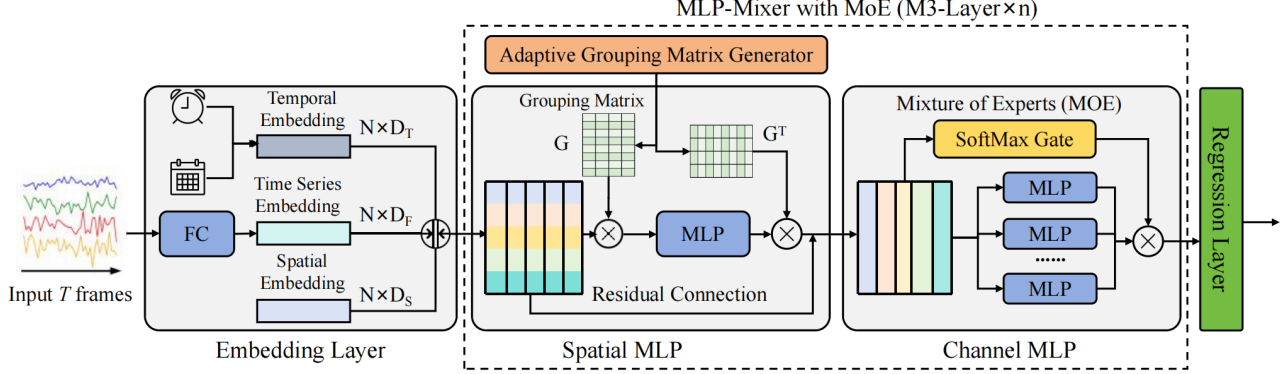


Figure 2: The framework of M3-Net.

to predict the traffic flow of the next 12 time steps, and record the prediction performance of the 3rd, 6th, 12th steps and the average. Our model is implemented by Pytorch 1.7 with vGPU-32GB. We set the number of spatial groups as 10 in spatial MLP, the number of experts in channel MLP as 4 and the number of M3-Layers as 3 by default. The dimension of hidden representations in our model is set as 128 and the dimension of embedding layer is set as 32. We set the Adam optimizer with an initial learning rate of 0.002, where the learning rate follows a step-wise decay strategy, and the batch size is set as 64.

Table 1: The description of the datasets in the experiments.

Dataset	Nodes	Edges	Time Range	Frames
PEMS03	358	546	09/01/2018 – 11/30/2018	26,208
PEMS04	307	338	01/01/2018 – 02/28/2018	16,992
PEMS07	883	865	05/01/2017 – 08/06/2017	28,224
PEMS08	170	276	07/01/2016 – 08/31/2016	17,856

3.2 Performance Evaluation

We compare our proposed model with fourteen state-of-art baselines as follows: DCRNN [11], STGCN [22], GWNNet [20], AGCRN [1], StemGNN [2], GMAN [24], MTGNN [18], DGCRN [9], STNorm [3] and STID [14]. The evaluation metrics are mean absolute errors (MAE), root mean squared errors (RMSE) and mean absolute percentage errors (MAPE) averaged over five times for one hour ahead prediction. The comparison results of our proposed model with other baselines on normal datasets are shown in Table 2. We can observe that our model achieves the best results on most metrics across multiple datasets and also achieves the second-best results on the remaining metrics. Baselines such as GWNNet, MTGNN, AGCRN, StemGNN and DGCRN are commonly used state-of-the-art models based on adaptive graphs in the field of ST prediction. The overall performance of M3-Net surpasses these models, demonstrating that the combination of the spatio-temporal embeddings and a finely designed MLP architecture can outperform some more complexly designed models.

3.3 Ablation Study

We conduct ablation study on PEMS04 and PEMS08 to evaluate the effectiveness of each crucial module in our model. As shown

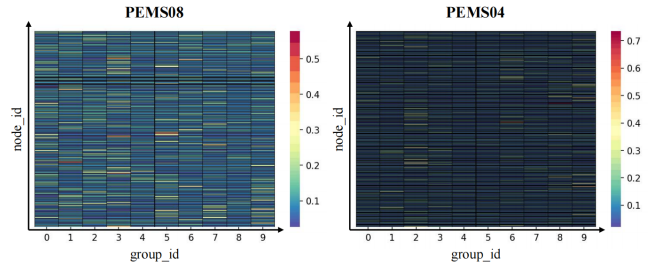


Figure 3: Adaptive grouping matrices visualization on PEMS04 and PEMS08.

in Table 3, we compared M3-Net with following ablation variants: 1) w/o MOE, which removes the mixture of experts mechanism from channel MLP module 2) w/o Spatial MLP, which removes the spatial MLP module from our model. 3) w/o Group Matrix, which removes the adaptive grouping matrix from spatial MLP module.

From Table 3, we can find that our complete model M3-Net outperforms all the ablation variants. The comparison of w/o MOE can demonstrate that capturing multi-scale spatio-temporal dependencies of traffic flow in road networks can be beneficial for predictive performance. The variant of w/o Spatial MLP can illustrate that the spatial MLP can capture the spatial correlations in historical traffic sequences for more accurate prediction. To further investigate the effectiveness of adaptive group matrix, we compare M3-Net with w/o Grouping Matrix. This comparison indicates that capturing spatial homogeneity is crucial for prediction performance.

3.4 Spatial Homogeneity Visualization

To further investigate how our proposed model characterizes the spatial homogeneity by the adaptive grouping matrix, we visualize the learned matrices on PEMS04 and PEMS08 by heatmaps. As shown in Fig. 3, the vertical axis represents the index of spatial nodes, and the horizontal axis represents the index of groups. In the heatmaps, colors closer to warm tones in each cell indicate a higher compatibility between a node and a group, whereas colors closer to cool tones indicate lower compatibility. It is easy to observe that the compatibility of some nodes with certain groups significantly exceeds the average value. Therefore, the adaptive grouping matrices effectively learn spatial homogeneity features.

Table 2: Performance comparisons on normal datasets. We bold the best-performing results and underline the suboptimal results.

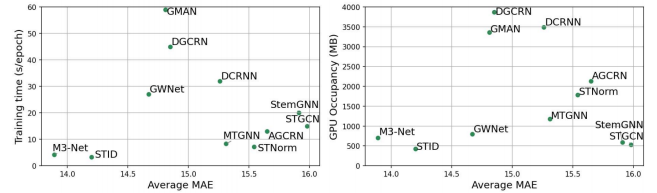
Dataset		PEMS04				PEMS07				PEMS08				PEMS03			
Method	Metric	@3	@6	@12	Avg.	@3	@6	@12	Avg.	@3	@6	@12	Avg.	@3	@6	@12	Avg.
DCRNN	MAE	18.53	19.65	21.67	19.71	19.45	21.18	24.14	21.20	14.16	15.24	17.70	15.26	14.41	15.52	16.77	15.54
	RMSE	29.61	31.37	34.19	31.43	31.39	34.42	38.84	34.43	22.20	24.26	27.14	24.28	25.10	27.15	29.63	27.18
	MAPE	12.71%	13.45%	15.03%	13.54%	8.29%	9.01%	10.42%	9.06%	9.31%	9.90%	11.13%	9.96%	14.43	15.58%	17.24%	15.62%
STGCN	MAE	18.74	19.64	21.12	19.63	20.33	21.66	24.16	21.71	14.95	15.92	17.65	15.98	14.85	15.79	17.79	15.83
	RMSE	29.84	31.34	33.53	31.32	32.73	35.35	39.48	35.41	23.48	25.36	28.03	25.37	25.67	27.48	30.16	27.51
	MAPE	14.42%	13.27%	14.22%	13.32%	8.68%	9.16%	10.26%	9.25%	9.87%	10.42%	11.34%	10.43%	14.62%	16.11%	17.67%	16.13%
GWNet	MAE	18.00	18.96	20.53	18.97	18.69	20.26	22.79	20.25	13.72	14.67	16.15	14.67	13.51	14.68	15.71	14.63
	RMSE	28.83	30.33	32.54	30.32	30.69	33.37	37.11	33.32	21.71	23.50	25.95	23.49	23.41	25.32	27.94	25.24
	MAPE	13.64%	14.23%	15.41%	14.26%	8.02%	8.56%	9.73%	8.63%	8.80%	9.49%	10.74%	9.52%	14.32%	15.63%	17.03%	15.52%
AGCRN	MAE	18.52	19.45	20.64	19.36	19.31	20.70	22.74	20.64	14.51	15.66	17.49	15.65	14.13	15.23	16.58	15.24
	RMSE	29.79	31.45	33.31	31.28	31.68	34.52	37.94	34.39	22.87	25.00	27.93	24.99	24.32	26.47	28.52	26.65
	MAPE	12.31%	12.82%	13.74%	12.81%	8.18%	8.66%	9.71%	8.74%	9.34%	10.34%	11.72%	10.17%	14.75%	15.92%	17.11%	15.89%
StemGNN	MAE	19.48	21.40	24.90	21.61	19.74	22.07	26.20	22.23	14.49	15.84	18.10	15.91	15.86	16.91	18.10	16.95
	RMSE	30.74	33.46	38.29	33.80	32.32	36.16	42.32	36.46	23.02	25.38	28.77	25.44	26.25	28.54	30.13	28.52
	MAPE	13.84%	15.85%	19.50%	16.10%	8.27%	9.20%	11.00%	9.20%	9.73%	10.78%	12.50	10.90%	17.84%	19.51%	21.02%	19.61%
GMAN	MAE	18.27	18.81	20.01	18.83	19.25	20.33	22.25	20.43	13.80	14.62	15.72	14.81	14.03	15.17	16.20	15.14
	RMSE	29.35	30.85	31.32	30.93	31.20	33.30	36.40	33.30	22.88	24.12	26.47	24.19	24.65	26.23	28.95	26.15
	MAPE	12.66%	13.25%	13.40%	13.21%	8.21%	8.63%	9.48%	8.69%	9.41%	9.57%	10.56%	9.69%	14.31%	15.38%	16.98%	15.41%
MTGNN	MAE	18.65	19.48	20.96	19.50	19.23	20.83	23.60	20.94	14.30	15.25	16.80	15.31	13.74	14.97	16.01	14.92
	RMSE	30.13	32.02	34.66	32.00	31.15	33.93	38.10	34.03	22.55	24.41	26.96	24.42	23.60	25.82	28.26	25.53
	MAPE	13.32%	14.08%	14.96%	14.04%	8.55%	9.30%	10.10%	9.10%	10.56%	10.54%	10.90%	10.70%	13.87%	14.49%	16.40%	14.55%
DGCRN	MAE	18.85	20.04	22.32	20.29	19.03	20.41	22.58	20.44	13.79	14.81	16.39	14.85	13.76	14.93	16.04	14.95
	RMSE	29.95	32.07	36.28	32.55	30.74	33.27	36.74	33.25	21.91	23.83	26.34	23.84	23.71	25.78	28.31	25.62
	MAPE	12.92%	13.50%	14.61%	13.60%	8.16%	8.69%	9.63%	8.73%	9.13%	9.74%	11.02%	9.84%	14.17%	15.23%	16.98%	15.35%
STNorm	MAE	18.28	18.92	20.20	18.96	19.15	20.63	22.60	20.52	14.44	15.53	17.20	15.54	14.21	15.32	16.28	15.35
	RMSE	29.70	31.12	32.91	30.98	31.70	35.10	38.65	34.85	22.68	25.07	27.86	25.01	23.62	25.88	28.27	25.93
	MAPE	12.28%	12.71%	13.43	12.69%	8.26%	8.84%	9.60%	8.77%	9.32%	9.98%	11.30%	10.03%	13.85%	14.53%	16.36%	14.56%
STID	MAE	17.62	18.43	19.82	18.44	18.31	19.59	21.52	19.54	13.28	14.21	15.58	14.20	14.17	15.29	16.27	15.31
	RMSE	28.57	29.93	31.95	29.92	30.39	32.90	36.29	32.85	21.66	23.57	25.89	23.49	24.81	27.36	29.79	27.40
	MAPE	12.00%	12.52%	13.63%	12.58%	7.72%	8.30%	9.15%	8.25%	8.62%	9.24%	10.33%	9.28%	14.72%	16.43%	17.65%	16.40%
M3-Net	MAE	17.58	18.34	19.42	18.30	18.18	19.51	21.28	19.42	13.05	13.95	15.01	13.89	<u>13.69</u>	<u>14.92</u>	<u>15.86</u>	<u>14.88</u>
	RMSE	<u>28.82</u>	<u>30.13</u>	31.82	<u>30.15</u>	30.21	32.78	36.03	32.85	21.48	23.47	25.54	23.33	<u>23.58</u>	<u>25.77</u>	<u>28.19</u>	<u>25.49</u>
	MAPE	<u>12.10%</u>	12.44%	13.41%	12.53%	7.66%	8.20%	9.07%	8.21%	8.52%	9.14%	10.02%	9.17%	<u>13.98%</u>	<u>14.99%</u>	<u>16.82%</u>	<u>15.02%</u>

Table 3: Ablation experiments.

Dataset	Model&Variants	MAE	RMSE	MAPE
PEMS04	M3-Net	18.30	30.15	12.53%
	w/o MOE	18.39	30.36	12.67%
	w/o Spatial MLP	18.42	30.31	12.63%
	w/o Grouping Matrix	18.83	30.95	12.76%
PEMS08	M3-Net	13.89	23.33	9.17%
	w/o MOE	14.04	23.42	9.25%
	w/o Spatial MLP	14.10	23.45	9.23%
	w/o Grouping Matrix	13.95	23.51	9.21%

3.5 Cost-Effectiveness Analysis

Time consumption and GPU memory usage are two intuitive indicators reflecting the time and space complexity of different models. Based on these two indicators, we conducted a comparative analysis of the cost-effectiveness of the proposed model and other baseline models on PEMS08 dataset. As shown in Fig. 4, the horizontal axis represents the average MAE metric values of model predictions, while the vertical axis represents the training time per epoch and the GPU memory usage. The closer the scatter points are to the origin, the higher the cost-effectiveness of the model, indicating that it balances prediction accuracy with efficiency and deployment cost. Observing the experimental results, it is evident that the cost-effectiveness of M3-Net surpasses other baseline models in terms of training time and memory usage, especially outperforming some previous state-of-the-art models based on spatio-temporal graphs.

**Figure 4: Visualization of cost-effectiveness of deployment on PEMS08 dataset.**

4 CONCLUSION

In this paper, we propose M3-Net, a lightweight and effective graph-free Multilayer Perceptron model to address the critical need for accurate traffic prediction in intelligent transportation systems. The innovative MLP-Mixer architecture, enhanced with a mixture of experts mechanism, allows for the joint learning of spatial and channel dimensions in traffic flow data. The incorporation of adaptive grouped matrices within the spatial MLP module effectively reduces the complexity of spatial learning, facilitating a more streamlined and efficient model. The extensive experiments conducted on various real-world datasets validate the effectiveness of M3-Net, demonstrating its superior performance in traffic prediction while maintaining a lightweight and deployable structure. Future work will explore further enhancements to the M3-Net architecture and its applicability to other domains within transportation and urban planning.

5 GenAI Usage Disclosure

None of the text, data, and code associated with this paper was produced by generative AI. We only used generative AI for language polishing.

References

- [1] Lei Bai, Lina Yao, Can Li, Xianzhi Wang, and Can Wang. 2020. Adaptive graph convolutional recurrent network for traffic forecasting. *Advances in neural information processing systems* 33 (2020), 17804–17815.
- [2] Defu Cao, Yujing Wang, Juanyong Duan, Ce Zhang, Xia Zhu, Congrui Huang, Yunhai Tong, Bixiong Xu, Jing Bai, Jie Tong, et al. 2020. Spectral temporal graph neural network for multivariate time-series forecasting. *Advances in neural information processing systems* 33 (2020), 17766–17778.
- [3] Jinliang Deng, Xiusi Chen, Renhe Jiang, Xuan Song, and Ivor W Tsang. 2021. St-norm: Spatial and temporal normalization for multi-variate time series forecasting. In *Proceedings of the 27th ACM SIGKDD conference on knowledge discovery & data mining*. 269–278.
- [4] Shengnan Guo, Youfang Lin, Ning Feng, Chao Song, and Huaiyu Wan. 2019. Attention based spatial-temporal graph convolutional networks for traffic flow forecasting. In *Proceedings of the AAAI conference on artificial intelligence*, Vol. 33. 922–929.
- [5] Guangyin Jin, Fuxian Li, Jinlei Zhang, Mudan Wang, and Jincai Huang. 2022. Automated dilated spatio-temporal synchronous graph modeling for traffic prediction. *IEEE Transactions on Intelligent Transportation Systems* 24, 8 (2022), 8820–8830.
- [6] Guangyin Jin, Yuxuan Liang, Yuchen Fang, Zezhi Shao, Jincai Huang, Junbo Zhang, and Yu Zheng. 2023. Spatio-temporal graph neural networks for predictive learning in urban computing: A survey. *IEEE Transactions on Knowledge and Data Engineering* 36, 10 (2023), 5388–5408.
- [7] Guangyin Jin, Lingbo Liu, Fuxian Li, and Jincai Huang. 2023. Spatio-temporal graph neural point process for traffic congestion event prediction. In *Proceedings of the AAAI conference on artificial intelligence*, Vol. 37. 14268–14276.
- [8] Guokun Lai, Wei-Cheng Chang, Yiming Yang, and Hanxiao Liu. 2018. Modeling long-and short-term temporal patterns with deep neural networks. In *The 41st international ACM SIGIR conference on research & development in information retrieval*. 95–104.
- [9] Fuxian Li, Jie Feng, Huan Yan, Guangyin Jin, Fan Yang, Funing Sun, Depeng Jin, and Yong Li. 2023. Dynamic graph convolutional recurrent network for traffic prediction: Benchmark and solution. *ACM Transactions on Knowledge Discovery from Data* 17, 1 (2023), 1–21.
- [10] Fuxian Li, Huan Yan, Guangyin Jin, Yue Liu, Yong Li, and Depeng Jin. 2022. Automated spatio-temporal synchronous modeling with multiple graphs for traffic prediction. In *Proceedings of the 31st ACM international conference on information & knowledge management*. 1084–1093.
- [11] Yaguang Li, Rose Yu, Cyrus Shahabi, and Yan Liu. 2018. Diffusion Convolutional Recurrent Neural Network: Data-Driven Traffic Forecasting. In *International Conference on Learning Representations*.
- [12] Hangchen Liu, Zheng Dong, Renhe Jiang, Jiewen Deng, Jinliang Deng, Quan-jun Chen, and Xuan Song. 2023. Spatio-temporal adaptive embedding makes vanilla transformer sota for traffic forecasting. In *Proceedings of the 32nd ACM international conference on information and knowledge management*. 4125–4129.
- [13] Xu Liu, Yutong Xia, Yuxuan Liang, Junfeng Hu, Yiwei Wang, Lei Bai, Chao Huang, Zhengguang Liu, Bryan Hooi, and Roger Zimmermann. 2023. Largest: A benchmark dataset for large-scale traffic forecasting. *Advances in Neural Information Processing Systems* 36 (2023), 75354–75371.
- [14] Zezhi Shao, Zhao Zhang, Fei Wang, Wei Wei, and Yongjun Xu. 2022. Spatial-temporal identity: A simple yet effective baseline for multivariate time series forecasting. In *Proceedings of the 31st ACM international conference on information & knowledge management*. 4454–4458.
- [15] Alex Sherstinsky. 2020. Fundamentals of recurrent neural network (RNN) and long short-term memory (LSTM) network. *Physica D: Nonlinear Phenomena* 404 (2020), 132306.
- [16] Chao Song, Youfang Lin, Shengnan Guo, and Huaiyu Wan. 2020. Spatial-temporal synchronous graph convolutional networks: A new framework for spatial-temporal network data forecasting. In *Proceedings of the AAAI conference on artificial intelligence*, Vol. 34. 914–921.
- [17] Ashish Vaswani, Noam Shazeer, Niki Parmar, Jakob Uszkoreit, Llion Jones, Aidan N Gomez, Łukasz Kaiser, and Illia Polosukhin. 2017. Attention is all you need. *Advances in neural information processing systems* 30 (2017).
- [18] Zonghan Wu, Shirui Pan, Guodong Long, Jing Jiang, Xiaojun Chang, and Chengqi Zhang. 2020. Connecting the dots: Multivariate time series forecasting with graph neural networks. In *Proceedings of the 26th ACM SIGKDD international conference on knowledge discovery & data mining*. 753–763.
- [19] Zonghan Wu, Shirui Pan, Guodong Long, Jing Jiang, and Chengqi Zhang. 2019. Graph wavenet for deep spatial-temporal graph modeling. *arXiv preprint arXiv:1906.00121* (2019).
- [20] Zonghan Wu, Shirui Pan, Guodong Long, Jing Jiang, and Chengqi Zhang. 2019. Graph wavenet for deep spatial-temporal graph modeling. In *Proceedings of the 28th International Joint Conference on Artificial Intelligence*. 1907–1913.
- [21] Mingxing Xu, Wenrui Dai, Chunmiao Liu, Xing Gao, Weiyao Lin, Guo-Jun Qi, and Hongkai Xiong. 2020. Spatial-temporal transformer networks for traffic flow forecasting. *arXiv preprint arXiv:2001.02908* (2020).
- [22] Bing Yu, Haoteng Yin, and Zhanxing Zhu. 2018. Spatio-temporal graph convolutional networks: a deep learning framework for traffic forecasting. In *Proceedings of the 27th International Joint Conference on Artificial Intelligence*. 3634–3640.
- [23] Yong Yu, Xiaosheng Si, Changhua Hu, and Jianxun Zhang. 2019. A review of recurrent neural networks: LSTM cells and network architectures. *Neural computation* 31, 7 (2019), 1235–1270.
- [24] Chuanpan Zheng, Xiaoliang Fan, Cheng Wang, and Jianzhong Qi. 2020. Gman: A graph multi-attention network for traffic prediction. In *Proceedings of the AAAI conference on artificial intelligence*, Vol. 34. 1234–1241.